nature nanotechnology

LETTERS

PUBLISHED ONLINE: 17 JUNE 2012 | DOI: 10.1038/NNANO.2012.90

Magnetoferritin nanoparticles for targeting and visualizing tumour tissues

Kelong Fan[1], Changqian Cao[2], Yongxin Pan[2], Di Lu[1], Dongling Yang[1], Jing Feng[1], Lina Song[1], Minmin Liang[1]* and Xiyun Yan[1]*

Engineered nanoparticles have been used to provide diagnostic[1–3], therapeutic[4,5] and prognostic information[6,7] about the status of disease. Nanoparticles developed for these purposes are typically modified with targeting ligands (such as antibodies[8–10], peptides[11,12] or small molecules[13]) or contrast agents[14–16] using complicated processes and expensive reagents. Moreover, this approach can lead to an excess of ligands on the nanoparticle surface, and this causes non-specific binding[17–20] and aggregation of nanoparticles[18–20], which decreases detection sensitivity[17–20]. Here, we show that magnetoferritin nanoparticles (M-HFn) can be used to target and visualize tumour tissues without the use of any targeting ligands or contrast agents. Iron oxide nanoparticles are encapsulated inside a recombinant human heavy-chain ferritin (HFn) protein shell, which binds to tumour cells that overexpress transferrin receptor 1 (TfR1). The iron oxide core catalyses the oxidation of peroxidase substrates in the presence of hydrogen peroxide to produce a colour reaction that is used to visualize tumour tissues. We examined 474 clinical specimens from patients with nine types of cancer and verified that these nanoparticles can distinguish cancerous cells from normal cells with a sensitivity of 98% and specificity of 95%.

Ferritin is an iron storage protein composed of 24 subunits made up of the heavy-chain ferritin (HFn) and the light-chain ferritin. Ferritin is spherical, with an outer diameter of 12 nm and interior cavity diameter of 8 nm (ref. 21). The cavity has been used as a reaction chamber to synthesize highly crystalline and monodisperse nanoparticles through biomimetic mineralization within the protein shell[22–24]. Recently, it was shown that HFn binds to human cells via transferrin receptor 1 (TfR1)[25]. Because TfR1 is overexpressed in tumour cells, this receptor has been used as a targeting marker for tumour diagnosis and therapy[26–29].

Current HFn-based tumour detection methods rely on functionalization of HFn with recognition ligands[30,31] and signal molecules[31,32]. Previously, we have shown that iron oxide nanoparticles can catalyse the oxidation of peroxidase substrates in the presence of hydrogen peroxide to produce a colour reaction similar to that of natural peroxidases[33]. We hypothesize that magnetoferritin (M-HFn) nanoparticles generated by encapsulating iron oxide nanoparticles inside a HFn shell should be able to target TfR1 without any additional recognition ligands on their surface, and visualize tumour tissues through the peroxidase activity of the iron oxide core (Fig. 1a).

We expressed recombinant human HFn in *Escherichia coli*. After purification, the proteins were analysed by transmission electron microscopy (TEM). The HFn protein shells had a well-defined morphology and were monodisperse in size (Fig. 1b,c). After iron loading and oxidation, a well-defined iron oxide core with an average diameter of ~4.7 nm was synthesized within the HFn protein shell (Fig. 1d,e). The iron mineral core of M-HFn is composed of magnetite or maghemite, as characterized in our previous publication[34]. Cryoelectron transmission microscopy (cryoTEM) analysis showed that the mineral cores were clearly encapsulated within the HFn protein shells (Fig. 1b). Dynamic light scattering (DLS) and size-exclusion chromatography (SEC) results further confirmed that the M-HFn nanoparticles were monodispersed with an outer diameter of ~12–16 nm (Supplementary Fig. S1a), and the iron loading did not significantly perturb the overall protein cage architecture of HFn (Supplementary Fig. S1b,c).

M-HFn nanoparticles catalyses the oxidation of peroxidase substrates 3,3,5,5-tetramethylbenzidine (TMB) and di-azo-aminobenzene (DAB) in the presence of H_2O_2 to give a blue colour (Fig. 1f) and brown colour (Fig. 1g), respectively, confirming that M-HFn nanoparticles have peroxidase activity towards typical peroxidase substrates. The mineral phase composition of the iron core determines the peroxidase activity of the M-HFn, as is evident from Supplementary Fig. S2. M-HFn with mineral cores consisting of magnetite or maghemite[34] exhibited a much higher peroxidase activity when compared with natural holoferritin. The natural cores in holoferritin consist mainly of the hydrated iron oxide mineral ferrihydrite ($5Fe_2O_3{\cdot}9H_2O$)[35], which exhibits little peroxidase activity. Apoferritin, without a mineral core, exhibited no peroxidase activity.

The specificity of HFn binding to living cancer cells was investigated using human breast, colon and liver cancer cell lines and their corresponding xenograft tumours. HT-29 human colon cancer cells and SMMC-7721 human liver cancer cells express TfR1 at high levels, but MX-1 human breast cancer cells do not express this receptor (Fig. 2a). HFn bound to TfR1-positive HT-29 and SMMC-7721 cells, and their xenograft tumours, but not to TfR1-negative MX-1 or its xenograft tumour (Fig. 2b,c). The binding of HFn to TfR1-positive cells was saturable, and could be inhibited by adding an excess of unconjugated HFn (Supplementary Fig. S3a), showing that HFn binding is specific. The saturation binding curve and Scatchard analysis demonstrate that the K_d value for HFn is 50 nM (Supplementary Fig. S3b), indicating that HFn has a high affinity for TfR1. In addition, HFn showed significant binding to A375 melanoma cells, MDA-MB-231 breast cancer cells, K562 erythroleukemia cells, HeLa cervical cancer cells, SKOV-3 ovarian cancer cells, PC-3 prostate cancer cells, U251 glioblastoma cells, U937 histiocytic lymphoma cells, SW1990 pancreatic cancer cells and Jurkat T-cell leukemia cells (Supplementary Fig. S4), indicating that HFn has a universal capability for recognizing cancer cells.

[1]Key Laboratory of Protein and Peptide Pharmaceutical, National Laboratory of Biomacromolecules, CAS-University of Tokyo Joint Laboratory of Structural Virology and Immunology, Institute of Biophysics, Chinese Academy of Sciences, 15 Datun Road, Beijing 100101, China, [2]Paleomagnetism and Geochronology Laboratory, Key Laboratory of the Earth's Deep Interior, Institute of Geology and Geophysics, Chinese Academy of Sciences, Beijing 100029, China. *e-mail: mmliang@moon.ibp.ac.cn; yanxy@sun5.ibp.ac.cn

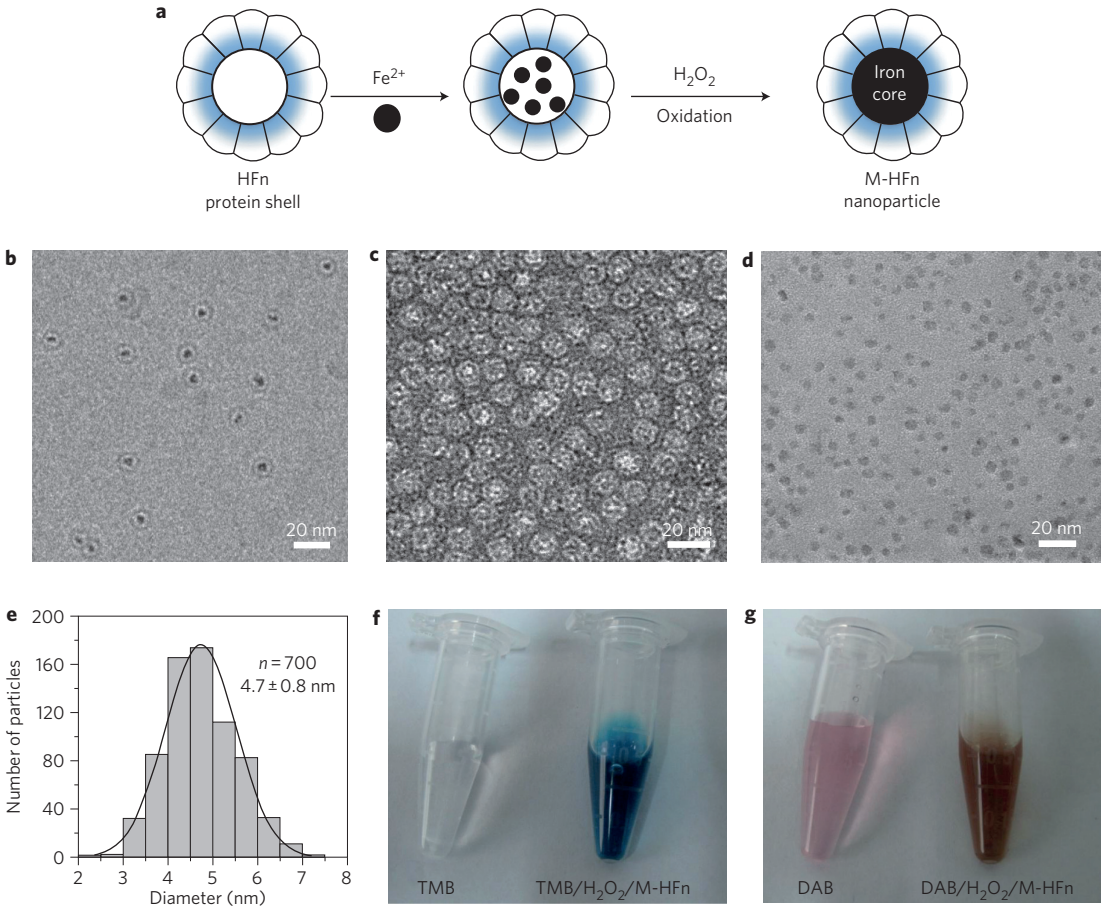

Figure 1 | Preparation and characterization of M-HFn nanoparticles. a, Schematic showing the preparation of M-HFn nanoparticles and their structure. **b**, CryoTEM image of M-HFn nanoparticles. **c**,**d**, TEM images of HFn protein shells (**c**) and iron oxide cores (**d**). HFn protein shells were negatively stained with uranyl acetate for TEM observations and iron oxide cores in HFn were unstained. **e**, Size distribution of iron oxide cores, with a median diameter of 4.7±0.8 nm. **f**,**g**, Characterization of peroxidase activity of M-HFn nanoparticles. M-HFn catalysed the oxidation of peroxidase substrates TMB (**f**) and DAB (**g**) in the presence of H_2O_2 to give a coloured product.

To investigate whether TfR1 mediates the specific binding of HFn to cancer cells, TfR1 was immunoprecipitated from HT-29 cell lysates. HFn reacted with the precipitated TfR1 (Fig. 2d), indicating that HFn binds to cancer cells via TfR1. The next far-Western blotting analysis showed that HFn bound to TfR1 in HT-29 and SMMC-7721 cells, but not in MX-1 cells (Fig. 2e), consistent with their TfR1 expression patterns (Fig. 2a) and confirming that TfR1 is the receptor of HFn and mediates its specific binding to cancer cells. Further flow cytometry and confocal results showed that anti-TfR1 monoclonal antibody (mAb) could completely inhibit the binding of FITC-labelled HFn to TfR1 on SMMC-7721 cancer cells (Supplementary Fig. S5), indicating that TfR1 is the only receptor for HFn present on these cancer cells. In addition, although transferrin competed with HFn for binding to TfR1, excess transferrin only partially inhibited HFn binding (Supplementary Fig. S6), consistent with observations reported by Li and Seaman[25]. These results suggest that HFn and transferrin share receptor TfR1, but may bind to different epitopes on TfR1.

To establish the validity of the M-HFn nanoparticle-based cancer diagnostic method, we carried out the following histological staining experiments in xenograft tumours. FITC-conjugated HFn showed strong fluorescence staining in HT-29, SKOV-3 and SMMC-7721 xenograft tumours (Fig. 3, top row), confirming the tumour-binding reactivity of the HFn protein. After iron loading and oxidation, M-HFn nanoparticles displayed an intensive brown peroxidase activity that visualized the tumour cells after adding DAB substrate and H_2O_2 (Fig. 3, middle row), verifying the feasibility of our M-HFn nanoparticle-based cancer diagnostic method. The fluorescence staining co-localized with mineral-peroxidase staining in tumour cells (Supplementary Fig. S7), indicating that iron loading and fluorescence labelling do not affect the tumour-binding activity of the HFn protein. This again shows the feasibility of our M-HFn-based assay for tumour detection.

Traditional immunohistochemical staining using anti-TfR1 antibodies (Abs) was next performed to compare its tumour-binding specificity and staining quality with our M-HFn nanoparticle-based method in xenograft tumour tissues. The intensity and the pattern of M-HFn nanoparticle-based staining were almost the same as that of immunohistochemical staining (Fig. 3, bottom row), demonstrating the accuracy of tumour detection by the M-HFn nanoparticles. TfR1-negative MX-1 tumour xenograft tissues consistently showed negative staining for M-HFn nanoparticles, FITC-conjugated HFn and TfR1 Abs (Fig. 3, right column), further confirming that HFn targets tumour cells via TfR1.

To evaluate the potential clinical application of M-HFn nanoparticles as a diagnostic agent for tumours in tissue specimens, we screened 247 clinical tumour tissue samples and 227 corresponding normal tissue samples by histological staining. Staining was considered positive when 10% or more of the tumour cells were stained (cutoff, 10%). M-HFn did not stain, or only slightly stained, normal or lesion tissues, with a staining frequency of only 4.8% (11/227, Table 1, Fig. 4). In tumour tissues, M-HFn

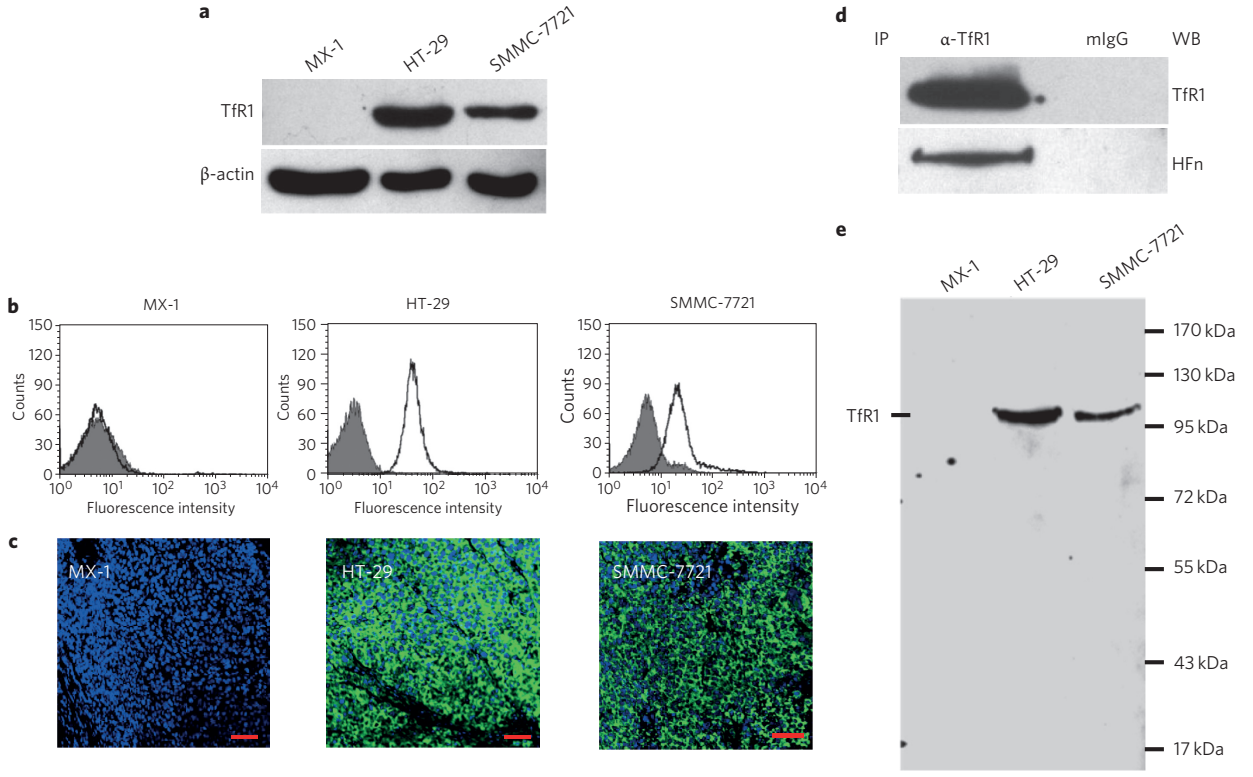

Figure 2 | HFn binds specifically to TfR1 in cancer cells. a, Western blot of TfR1 expression in HT-29 colon cancer cells, SMMC-7721 liver cancer cells and MX-1 breast cancer cells. β-actin was used as a loading control. **b**, Flow cytometric analysis of the specific binding of HFn to HT-29, SMMC-7721 and MX-1 cancer cells. **c**, Fluorescence staining of HT-29, SMMC-7721 and MX-1 xenograft tumours incubated with FITC-conjugated HFn (scale bars, 50 μm). **d**, TfR1 immunoprecipitated from HT-29 cell lysates by anti-TfR1 mAbs (α-TfR1) was recognized by HFn, detected by mouse anti-HFn mAbs and visualized with HRP-coupled anti-mouse IgG. **e**, Far-Western blotting of HT-29, SMMC-7721 and MX-1 cell line lysates was performed using HFn, detected by mouse anti-HFn mAbs and visualized with HRP-coupled anti-mouse IgG. TfR1 represented an ~95 kDa band.

nanoparticles strongly stained tumour cells, and a clear distinction was seen between cancerous cells and adjacent normal cells in representative sections (Fig. 4). M-HFn staining showed a sensitivity of 98% across nine types of cancer represented by 247 tumour tissues (Table 1). These clinical tissue specimens were further stained with FITC-conjugated HFn protein shells. As expected, consistent staining patterns were observed (Fig. 4), verifying the diagnosis based on M-HFn nanoparticles. Importantly, HFn showed a distinct staining reaction in different grades and growth patterns of hepatocellular carcinoma, lung squamous cell carcinoma, cervical squamous cell carcinoma, prostate adenocarcinoma, ovarian serous papillary carcinoma and colonic adenocarcinoma (Supplementary Fig. S8–S13), demonstrating that HFn has an impressive ability to discriminate tumour cells from normal cells, and thus has clinical potential in cancer diagnosis.

To understand the mechanism of the M-HFn-based peroxidase-like reaction, the formation of $OH^{\bullet}$ during the reaction was measured using electron spin resonance. $OH^{\bullet}$ was produced during the peroxidase-like reaction in the presence of both M-HFn nanoparticles and H_2O_2 (Supplementary Fig. S14a,b). With the addition of an $OH^{\bullet}$ scavenger (ethanol), the formed $OH^{\bullet}$ disappeared (Supplementary Fig. S14 c) and the peroxidase activity of the M-HFn nanoparticles decreased to 20% of the original activity (Supplementary Fig. S14d,e), indicating that the $OH^{\bullet}$ formed during the peroxidase-like reaction is responsible for the catalytic oxidation of peroxidase substrate that gives the coloured precipitate at the site of its target.

Based on these results, we propose the following reaction mechanism. With the addition of H_2O_2 and peroxidase substrate to the M-HFn reaction solution, H_2O_2 diffuses into the ferritin cavity through its hydrophilic channels and interacts with the iron oxide core of M-HFn to generate $OH^{\bullet}$ on the surface of the iron core. The generated $OH^{\bullet}$ then oxidizes nearby peroxidase substrates (for example, DAB) to form an insoluble coloured precipitate at the site of the M-HFn, which is targeted to cancer cells. The coloured precipitates are only formed at the site of the M-HFn because $OH^{\bullet}$ radicals are highly reactive and short-lived, and can only oxidize nearby substrates. The clear boundary between tumour and normal tissues on M-HFn-stained tissue slides (Supplementary Fig. S15) also demonstrates that the coloured precipitates are generated right at the site of the M-HFn-targeted cancer cells and do not diffuse away from their targets.

Achieving rapid, low-cost and sensitive cancer diagnosis remains a challenge due to the complexities of this disease. Our studies show that one-step tumour targeting and visualization with low-cost and mass-produced M-HFn nanoparticles is feasible for convenient and sensitive monitoring and analysis of tumour cells in tissue specimens. The recombinant human HFn protein shell has tumour-specific binding properties, and the encapsulated iron oxide core has strong peroxidase activity, which allows us to combine effective tumour cell recognition in clinical tissues with highly sensitive staining of the targeted cells. Staining results for 247 clinical tumour tissue samples from patients with ovarian, liver, prostate, lung, breast, cervical, thymus colorectal or oesophageal cancers, as well as for 227 normal and lesion tissue control samples (Table 1, Fig. 4), clearly demonstrate the capacity of M-HFn nanoparticles to distinguish cancer cells from normal ones in tissue specimens.

Compared with conventional antibody-based histological methods for cancer detection in clinics, our novel M-HFn nanoparticle-based method has the following advantages. First, it has high

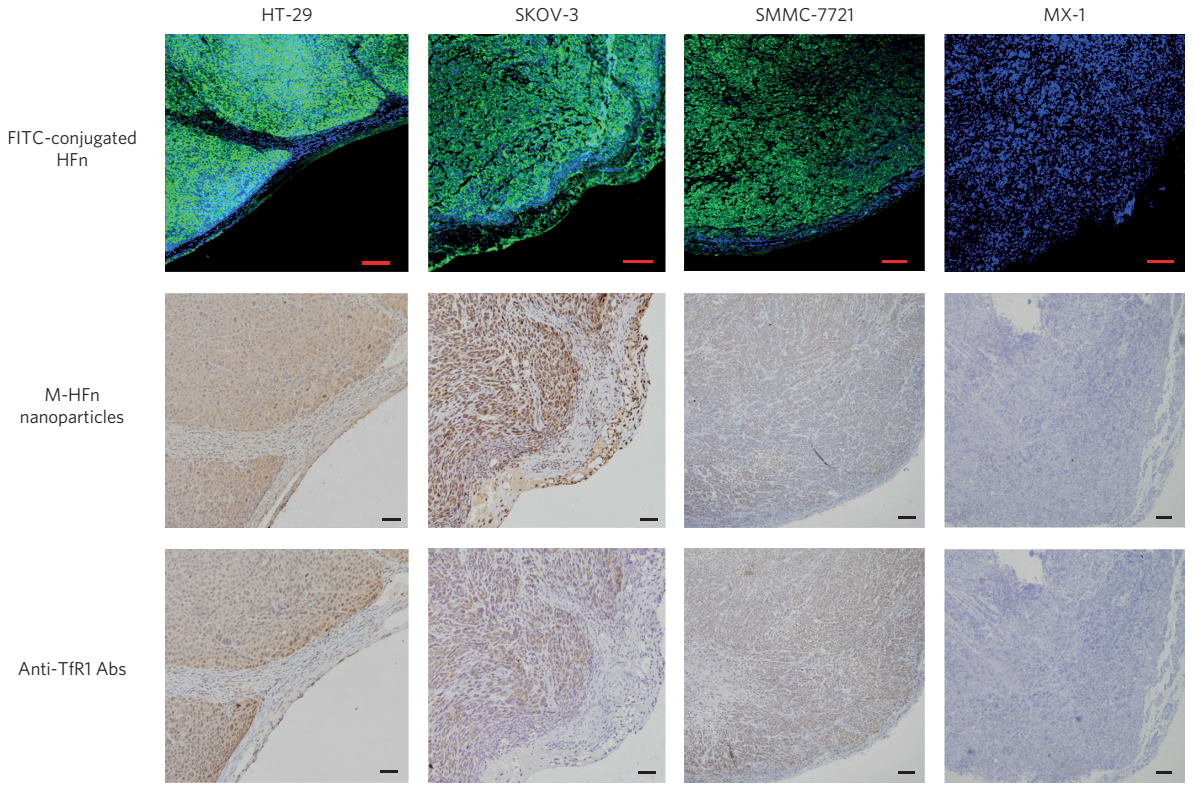

Figure 3 | M-HFn nanoparticle staining of tumour tissues. FITC-conjugated HFn-based fluorescence staining (top row), M-HFn nanoparticle-based peroxidase staining (middle row) and anti-TfR1 Abs-based immunohistochemical staining (bottom row) of paraffin-embedded HT-29 colon cancer, SKOV-3 ovarian cancer, SMMC-7721 liver cancer and MX-1 breast cancer xenograft tumours. TfR1-positive xenograft tumours showed strong positive staining for FITC-conjugated HFn (green fluorescence), M-HFn nanoparticles (brown) and anti-TfR1 Abs (brown), whereas TfR1-negative xenograft tumours showed no staining for FITC-conjugated HFn, M-HFn nanoparticles and anti-TfR1 Abs (scale bars, 100 μm). Abs, antibodies.

sensitivity and specificity. Screening 474 clinical specimens from patients with nine types of cancer shows that the M-HFn nanoparticle-based method has a sensitivity of 98% and a specificity of 95% (Table 1), which is much better than most antibody-based histological detection methods reported in the literature (Supplementary Table S1). In addition, a side-by-side comparison of the standard antibody-based immunohistochemistry and our M-HFn-based approach in two hepatocellular carcinoma cases identified by pathologists also shows that our M-HFn-based approach performs much better than anti-TfR1 antibody-based immunohistochemistry when distinguishing tumours from normal tissues (Supplementary Fig. S16). The second advantage of our method is its high accuracy, credibility and repeatability. Traditional immunohistochemistry involves multiple manipulation steps. The results are easily affected by the proficiency and subjectivity of the manipulators. By using a one-step incubation of one reagent in our M-HFn nanoparticle-based method, the accuracy, credibility and repeatability of the results are improved greatly. Our method also has the advantage of a rapid examination time, taking 1 h, rather than the 4 h required for immunohistochemistry, which generally involves multistep incubation of primary antibody, secondary antibody or enzyme-labelled third antibody. Finally, it is low in cost, avoiding the use of expensive and unstable antibodies, and the HFn can be produced in *Escherichia coli* at high yield. M-HFn nanoparticles can be low in cost and mass-produced by simply oxidizing Fe^{2+} within HFn by H_2O_2.

M-HFn-based peroxidase staining and FITC-HFn-based fluorescence staining target tumour cells via the same HFn protein, but visualize them using chromogenic and fluorescence signals, respectively. Peroxidase staining is clearly better for clinical diagnostics because it is compatible with haematoxylin counterstains, which allows visualization of the context of a tumour's expression pattern and provides more detailed histopathological information, allowing diagnostic features to be easily discerned. Fluorescence staining, as with most fluorescence techniques, has two significant

Table 1 | Histological analysis of M-HFn nanoparticle staining of tumours in clinical tissue specimens.

Tumour tissues	Positive/cases (sensitivity)	Normal tissues	Negative/cases (specificity)
Hepatocellular carcinoma	54/55 (98%)	Liver	39/45 (87%)
Lung squamous cell carcinoma	50/52 (96%)	Lung	55/56 (98%)
Colonic adenocarcinoma	23/23 (100%)	Colon	40/41 (98%)
Cervical squamous cell carcinoma	28/28 (100%)	Cervix	52/52 (100%)
Prostate adenocarcinoma	22/22 (100%)	Prostate	14/16 (88%)
Ovarian serous papillary carcinoma	55/56 (98%)	Ovary	4/4 (100%)
Breast ductal carcinoma	3/4 (75%)	Breast	4/4 (75%)
Thymic carcinoma	4/4 (100%)	Thymus	4/4 (100%)
Oesophagus squamous cell carcinoma	2/3 (67%)	Oesophagus	5/5 (100%)
Total	241/247 (98%)	Total	216/227 (95%)

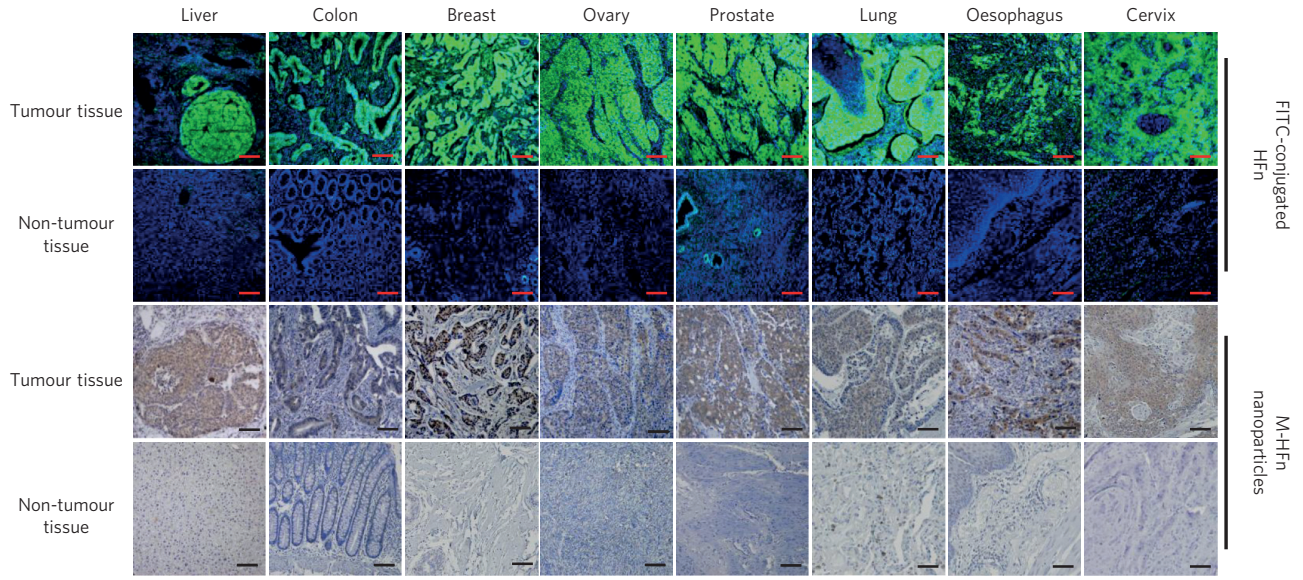

Figure 4 | Cancer diagnosis in clinical specimens using M-HFn nanoparticles. Paraffin-embedded clinical tumour tissues, and their corresponding normal and lesion tissues, were stained by FITC-conjugated HFn protein shells and M-HFn nanoparticles. Tumour tissues showed strong positive staining for M-HFn nanoparticles (brown) and FITC-conjugated HFn protein shells (green fluorescence), whereas the normal and lesion tissue controls were negative for M-HFn nanoparticles and FITC-conjugated HFn. Scale bars, 100 μm.

problems—photobleaching and autofluorescence—which severely limits the detection sensitivity of FITC-HFn-based fluorescence staining. This study suggests that the easily synthesized M-HFn nanoparticles have the potential to become a diagnostic tool for rapid, low-cost and universal assessment of cell cancerization.

Methods

Conjugation of HFn and M-HFn. HFn and M-HFn were labelled by fluorescein isothiocyanate (FITC, Sigma) using the following procedure. FITC was dissolved in dry dimethylformamide and added to an HFn or M-HFn solution in 0.1 M $NaHCO_3$, pH 8.5, at an FITC to HFn or M-HFn molar ratio of 10:1. The reaction solution was gently stirred for 3 h at room temperature in the dark and then purified on a polyacrylamide column (Thermo Scientific, MWCO 6000) using 0.1 M PBS, pH 7.5, as an eluant to remove free dyes. The labelled FITC concentration was determined by measuring the absorbance at 492 nm, and the HFn or M-HFn concentration was determined using a BCA protein assay reagent kit.

Cell binding studies. The reactivity of HFn with cancer cell lines was assessed by flow cytometry. Briefly, 100 μl detached cell suspensions (1×10^6 cells per ml) were stained with 20 μg ml^{-1} of FITC-conjugated HFn for 2 h at 4 °C in PBS containing 0.3% bovine serum albumin. After three washes in cold PBS, cells were analysed immediately using a FACSCalibur flow cytometry system (Becton Dickinson).

Western blotting, far-Western blotting and immunopreciptation. TfR1 expression was assessed by Western blotting. Cell lysates of each type were run on a 10% SDS–polyacrylamide gel and transferred to a nitrocellulose membrane blocked with 5% non-fat milk, 0.1% Tween 20 in PBS for 30 min, and then incubated overnight at 4 °C with a 1:2,000 dilution of mouse anti-human TfR1 monoclonal antibody (mAbs, BD Bioscience). The TfR1 mAbs was detected using a 1:6,000 dilution of goat anti-mouse IgG conjugated to HRP (Pierce), and developed with ECL substrate (Pierce).

Immunopreciptation was performed to confirm that TfR1 is the binding receptor of HFn. Cell lysates were pre-cleared by incubation with 15 μl protein A/G agarose (Santa Cruz Biotech), centrifuged to remove the beads, and then incubated at 4 °C overnight with 4 μl of 0.5 mg ml^{-1} mouse anti-human TfR1 mAbs or 1 μl of 2 mg ml^{-1} normal mouse IgG (Sigma) as a control, followed by incubation with 15 μl protein A/G agarose for 1 h at room temperature. The precipitated complexes were boiled for 15 min, analysed by 10% SDS–polyacrylamide gel and then transferred to a nitrocellulose membrane. After blocking with non-fat dry milk, the nitrocellulose membranes were probed with a 1:2,000 dilution of anti-TfR1 mAbs or with 3.8 μg ml^{-1} HFn protein followed by a 1:2,000 dilution of mouse anti-HFn mAbs, and developed with HRP-conjugated anti-mouse IgG.

Far-Western blotting was performed to analyse the binding pattern of HFn to cancer cells. Lysates from the HT-29, SMMC-7721 and MX-1 cell lines were run on a 10% SDS–polyacrylamide gel and transferred to a nitrocellulose membrane, blocked in non-fat dry milk for 30 min, and then incubated overnight at 4 °C with HFn (3.8 μg ml^{-1}). HFn was detected using a 1:2,000 dilution of mouse anti-HFn mAbs (Santa Cruz Biotech), and developed with HRP-conjugated anti-mouse IgG.

Staining of tumour xenografts and clinical specimens. Paraffin-embedded tissue sections were deparaffinized by washing twice in xylene for 10 min and then hydrated progressively using an ethanol gradient. Endogenous peroxidase activity was quenched by incubation with 0.3% H_2O_2 in methanol for 30 min. After rinsing, the tissue sections were boiled in 10 mM citrate buffer (pH 6.0) at 100 °C for 30 min, cooled to room temperature, blocked with 5% goat serum in PBS for 1 h at 37 °C, washed and then incubated with M-HFn nanoparticles (1.8 μM) for 1 h at 37 °C, and then rinsed in PBS. Freshly prepared DAB was added for colour development. All samples were counterstained with haematoxylin (blue stain). The stained sections were analysed under a microscope and the results were expressed in terms of the percentage of stained tumour cells (0 to 100%). If 10% or more of the tumour cells were stained, the slide was scored as positive. Two independent pathologists who were blind to all clinical information scored all specimens.

Fluorescence staining of tissue sections was performed to confirm the binding specificity of HFn to cells. After blocking in serum, tissue sections were incubated with FITC-conjugated HFn (1 μM) at 4 °C overnight. The stained tissues were examined under a confocal laser scanning microscope (Olympus).

Immunohistochemical staining of tissue sections by anti-TfR1 Abs was performed to compare tumour-binding specificity and staining quality with M-HFn nanoparticles. Briefly, after blocking in serum, tissue sections were incubated at 4 °C overnight with a 1:300 dilution of polyclonal rabbit anti-TfR1 antibody (Abcam). The bound antibody was detected by incubating the tissues with a 1:1,000 dilution of biotinylated anti-rabbit antibody (Santa Cruz Biotech) at 37 °C for 1 h, then with a 1:200 dilution of HRP-conjugated streptavidin (Pierce) for 40 min.

Received 27 February 2012; accepted 7 May 2012; published online 17 June 2012

References

1. Galanzha, E. I. *et al. In vivo* magnetic enrichment and multiplex photoacoustic detection of circulating tumour cells. *Nature Nanotech.* **4,** 855–860 (2009).
2. Winter, P. M. *et al.* Molecular imaging of angiogenesis in nascent Vx-2 rabbit tumors using a novel $\alpha_v\beta_3$-targeted nanoparticle and 1.5 tesla magnetic resonance imaging. *Cancer Res.* **63,** 5838–5843 (2003).
3. Stoeva, S. I., Lee, J. S., Smith, J. E., Rosen, S. T. & Mirkin, C. A. Multiplexed detection of protein cancer markers with biobarcoded nanoparticle probes. *J. Am. Chem. Soc.* **128,** 8378–8379 (2006).
4. Janib, S. M., Moses, A. S. & Mackay, J. A. Imaging and drug delivery using theranostic nanoparticles. *Adv. Drug Del. Rev.* **3,** 1–2 (2010).
5. Zrazhevskiy, P., Sena, M. & Gao, X. H. Designing multifunctional quantum dots for bioimaging, detection, and drug delivery. *Chem. Soc. Rev.* **3,** 1–2 (2010).
6. Li, R. L. *et al.* Prognostic value of Akt-1 in human prostate cancer: a computerized quantitative assessment with quantum dot technology. *Clin. Cancer Res.* **15,** 3568–3573 (2009).

7. Karathanasis, E. *et al.* Multifunctional nanocarriers for mammographic quantification of tumor dosing and prognosis of breast cancer therapy. *Biomaterials* **29,** 4815–4822 (2008).
8. Jaetao, J. E. *et al.* Enhanced leukemia cell detection using a novel magnetic needle and nanoparticles. *Cancer Res.* **69,** 8310–8316 (2009).
9. Corsi, F. *et al.* HER2 expression in breast cancer cells is downregulated upon active targeting by antibody-engineered multifunctional nanoparticles in mice. *ACS Nano* **5,** 6383–6393 (2011).
10. Xu, H. Y. *et al.* Antibody conjugated magnetic iron oxide nanoparticles for cancer cell separation in fresh whole blood. *Biomaterials* **32,** 9758–9765 (2011).
11. Park, Y. *et al.* A new atherosclerotic lesion probe based on hydrophobically modified chitosan nanoparticles functionalized by the atherosclerotic plaque targeted peptides. *J. Control. Rel.* **128,** 217–223 (2008).
12. Kumar, A. *et al.* Gold nanoparticles functionalized with therapeutic and targeted peptides for cancer treatment. *Biomaterials* **33,** 1180–1189 (2012).
13. Weissleder, R., Kelly, K., Sun, E. Y., Shtatland, T. & Josephson, L. Cell-specific targeting of nanoparticles by multivalent attachment of small molecules. *Nature Biotechnol.* **23,** 1418–1423 (2005).
14. Gao, X., Cui, Y., Levenson, R. M., Chung, L. W. & Nie, S. *In vivo* cancer targeting and imaging with semiconductor quantum dots. *Nature Biotechnol.* **22,** 969–976 (2004).
15. Michalet, X. *et al.* Quantum dots for live cells, *in vivo* imaging, and diagnostics. *Science* **307,** 538–544 (2005).
16. Jin, Y. D., Jia, C. X., Huang, S. W., O'Donnell, M. & Gao, X. H. Multifunctional nanoparticles as coupled contrast agents. *Nature Commun.* **1,** 1–8 (2010).
17. Chen, H. W. *et al.* Reducing non-specific binding and uptake of nanoparticles and improving cell targeting with an antifouling PEO-*b*-PγMPS copolymer coating. *Biomaterials* **31,** 5397–5407 (2010).
18. Bagwe, R. P., Hilliard, L. R. & Tan, W. Surface modification of silica nanoparticles to reduce aggregation and nonspecific binding. *Langmuir* **22,** 4357–4362 (2006).
19. Grubbs, R. B. Roles of polymer ligands in nanoparticle stabilization. *Polym. Rev.* **47,** 197–215 (2007).
20. Doshi, N. & Mitragotri, S. Designer biomaterials for nanomedicine. *Adv. Funct. Mater.* **19,** 3843–3854 (2009).
21. Theil, E. C. Ferritin-structure, gene-regulation, and cellular function in animals, plants, and microorganisms. *Annu. Rev. Biochem.* **56,** 289–315 (1987).
22. Meldrum, F. C., Heywood, B. R. & Mann, S. Magnetoferritin: *in vitro* synthesis of a novel magnetic protein. *Science* **257,** 522–523 (1992).
23. Douglas, T. & Young, M. Host–guest encapsulation of materials by assembled virus protein cages. *Nature* **393,** 152–155 (1998).
24. Allen, M., Willits, D., Mosolf, J., Young, M. & Douglas, T. Protein cage constrained synthesis of ferrimagnetic iron oxide nanoparticles. *Adv. Mater.* **14,** 1562–1565 (2002).
25. Li, L. *et al.* Binding and uptake of H-ferritin are mediated by human transferrin receptor-1. *Proc. Natl Acad. Sci. USA* **107,** 3505–3510 (2010).
26. Sutherland, R. *et al.* Ubiquitous cell-surface glycoprotein on tumor-cells is proliferation-associated receptor for transferrin. *Proc. Natl Acad. Sci. USA* **78,** 4515–4519 (1981).
27. Ryschich, E. *et al.* Transferrin receptor is a marker of malignant phenotype in human pancreatic cancer and in neuroendocrine carcinoma of the pancreas. *Eur. J. Cancer* **40,** 1418–1422 (2004).
28. Walker, R. A. & Day, S. J. Transferrin receptor expression in non-malignant and malignant human breast tissue. *J. Pathol.* **148,** 217–224 (1986).
29. Daniels, T. R., Delgado, T., Rodriguez, J. A., Helguera, G. & Penichet, M. L. The transferrin receptor part I: biology and targeting with cytotoxic antibodies for the treatment of cancer. *Clin. Immunol.* **121,** 144–158 (2006).
30. Uchida, M. *et al.* Targeting of cancer cells with ferrimagnetic ferritin cage nanoparticles. *J. Am. Chem. Soc.* **128,** 16626–16633 (2006).
31. Lin, X. *et al.* Chimeric ferritin nanocages for multiple function loading and multimodal imaging. *Nano Lett.* **11,** 814–819 (2011).
32. Lin, X. *et al.* Hybrid ferritin nanoparticles as activatable probes for tumor imaging. *Angew. Chem. Int. Ed.* **50,** 1569–1572 (2011).
33. Gao, L. Z. *et al.* Intrinsic peroxidase-like activity of ferromagnetic nanoparticles. *Nature Nanotech.* **2,** 577–583 (2007).
34. Cao, C. Q. *et al.* Magnetic characterization of noninteracting, randomly oriented, nanometer-scale ferrimagnetic particles. *J. Geophys. Res.* **115,** B07103 (2010).
35. Mann, S., Bannister, J. V. & Williams, R. J. Structure and composition of ferritin cores isolated from human spleen, limpet (*Patella vulgata*) hemolymph and bacterial (*Pseudomonas aeruginosa*) cells. *J. Mol. Biol.* **188,** 225–232 (1986).

Acknowledgements

This work was partially supported by grants from the National Science and Technology Major Project (2012ZX10002009-016), the Knowledge Innovation Program of the Chinese Academy of Sciences (KJCX2-YW-M15), 973 Program (2011CB933500, 2012CB934003), and the National Defense Science and Technology Innovation Fund of Chinese Academy of Sciences (CXJJ-11-M61).

Author contributions

M.L. conceived and designed the experiments. K.F. and M.L. performed the experiments. M.L. and X.Y. reviewed, analysed and interpreted the data. C.C. and Y.P. synthesized the nanoparticles. D.L., D.Y., J.F. and L.S. cultured the cancer cells. M.L. wrote the paper. All authors discussed the results and commented on the manuscript.

Additional information

The authors declare no competing financial interests. Supplementary information accompanies this paper at www.nature.com/naturenanotechnology. Reprints and permission information is available online at http://www.nature.com/reprints. Correspondence and requests for materials should be addressed to M.L. and X.Y.